The Astrophysical Journal, 643:200–209, 2006 May 20

STELLAR KINEMATICS FOR THE CENTRAL SPHEROID IN THE POLAR DISK GALAXY NGC 4650A[1]

E. Iodice,[2] M. Arnaboldi,[3,4] R. P. Saglia,[5] L. S. Sparke,[6] O. Gerhard,[5,7] J. S. Gallagher,[6] F. Combes,[8] F. Bournaud,[8] M. Capaccioli,[9,10] and K. C. Freeman[11]

Received 2005 November 15; accepted 2006 January 20

ABSTRACT

We have obtained high angular resolution, high signal-to-noise ratio spectra of the calcium triplet absorption lines on the photometric axes of the stellar spheroid in the polar disk galaxy NGC 4650A. Along the major axis, the observed rotation and velocity dispersion measurements show the presence of a kinematically decoupled nucleus and a flat velocity dispersion profile. The minor-axis kinematics is determined for the first time: along this direction some rotation is measured, and the velocity dispersion is nearly constant and slightly increases at larger distances from the center. The new high-resolution kinematic data suggest that the stellar component in NGC 4650A resembles a nearly exponential oblate spheroid supported by rotation. The main implications of these results on the previous mass models for NGC 4650A are discussed. Moreover, the new kinematic data set constraints on current models for the formation scenarios of polar ring galaxies, supporting a slow accretion rather than a secondary strong dissipative event.

Subject headings: galaxies: individual (NGC 4650A) — galaxies: kinematics and dynamics

Online material: color figure

1. INTRODUCTION

Studies of galaxy formation and evolution both in the Local Group and in the high-redshift universe (Conselice et al. 2003) provide increasing evidence that mergers play a role in the formation of early-type galaxies, in clusters and in the field (Schweizer 1999; Hibbard & Yun 1999). The merging of two disk galaxies produces a spheroidal remnant with physical properties, such as density profiles, mean velocity dispersion, and surface brightness, that are similar to those observed for elliptical and early-type disk galaxies (Toomre & Toomre 1972; Gerhard 1981; Barnes & Hernquist 1992; Bekki 1998b; Naab & Burkert 2003; Bournaud et al. 2005). These kinds of mergers may also produce a polar ring galaxy (PRG; Bekki 1998a; Bournaud & Combes 2003) such as NGC 4650A (Fig. 1).

PRGs generally contain a central featureless stellar spheroid and an elongated structure, the "polar ring," which in projection appears close to the inner spheroid's meridian plane. In all PRGs, the H I gas is associated with the polar structure and not with the central stellar spheroid; furthermore, the stars in the central spheroid and the gas and stars in the polar structure rotate in two nearly perpendicular planes. The studies of PRGs promise to yield detailed information about some of the processes at work during galaxy merging and on the shape of dark matter halos around galaxies (Schweizer et al. 1983; Sackett & Sparke 1990; Sackett et al. 1994; Combes & Arnaboldi 1996; Iodice et al. 2003).

NGC 4650A is the prototype for PRGs. Its luminous components, the inner spheroid and the polar structure, have been studied with optical and near-infrared (NIR) photometry, optical spectroscopy, and in the radio (H I 21 cm line and continuum). The surface brightness profile of the central spheroid is described by an exponential law, with a small exponential nucleus; its integrated optical versus NIR colors are similar to those of an intermediate-age stellar population (Iodice et al. 2002; Gallagher et al. 2002). Previous absorption-line spectroscopy at optical wavelengths showed a substantial rotation along the major axis, with $v_{\max} \simeq 100$ km s^{-1} (Whitmore et al. 1987; Sackett et al. 1994), while the velocity dispersion measurements were plagued by systematic errors, caused by both low angular and low spectral resolution. The best estimates gave $\sigma_0 \simeq 60$ km s^{-1}.

The polar structure in NGC 4650A has been shown to be a disk rather than a ring. Its stars and dust can be reliably traced inward within the stellar spheroid to $\sim$1.2 kpc radius from the galaxy nucleus (Iodice et al. 2002; Gallagher et al. 2002). Emission and absorption-line optical spectra show that it is an extended stellar disk rather than a narrow ring (Swaters & Rubin 2003): both rotation curves show a linear inner gradient and a plateau, as expected for a disk in differential rotation. Furthermore, the H I 21 cm observations (Arnaboldi et al. 1997) show that the gas is 5 times more extended than the luminous polar structure, with a position-velocity diagram very similar to those observed for edge-on gaseous disks.

The question about the shape of the dark halo of NGC 4650A is still open. Because of the large error bars in the velocity dispersion profile, dynamical models by Sackett et al. (1994) and

[1] Based on data collected with the FORS2 spectrograph, mounted at the UT4 of the Very Large Telescope at Cerro Paranal, Chile, operated by ESO, during observing run 70.B-0277.

[2] INAF–Osservatorio Astronomico di Capodimonte, via Moiariello 16, 80131 Napoli, Italy; iodice@na.astro.it.

[3] INAF–Osservatorio Astronomico di Torino, Strada Osservatorio 20, Pino Torinese, Italy; arnaboldi@to.astro.it.

[4] European Southern Observatory, Karl-Schwarzschild-Strasse 2, D-85748 Garching bei Munchen, Germany.

[5] Max-Planck-Institut für extraterrestrische Physik, Giessenbachstrasse, 85748 Garching, Germany; saglia@mpe.mpg.de.

[6] Department of Astronomy, University of Wisconsin, 475 North Charter Street, Madison, WI 53706.

[7] Astronomisches Institut, Universität Basel, Venusstrasse 7, CH-4102 Binningen, Switzerland.

[8] Observatoire de Paris, LERMA, 61 Avenue de l'Observatoire, 75014 Paris, France.

[9] Dipartimento di Scienze Fisiche, Università di Napoli Federico II, via Cintia ed. G, 80126 Napoli, Italy.

[10] VST Center at Naples (VSTceN), INAF–Osservatorio Astronomico di Capodimonte, Via Moiariello 16, 80131 Napoli, Italy.

[11] Mount Stromlo Observatory, Research School of Astronomy and Astrophysics, Cotter Road, Weston Creek, ACT 2611, Australia.

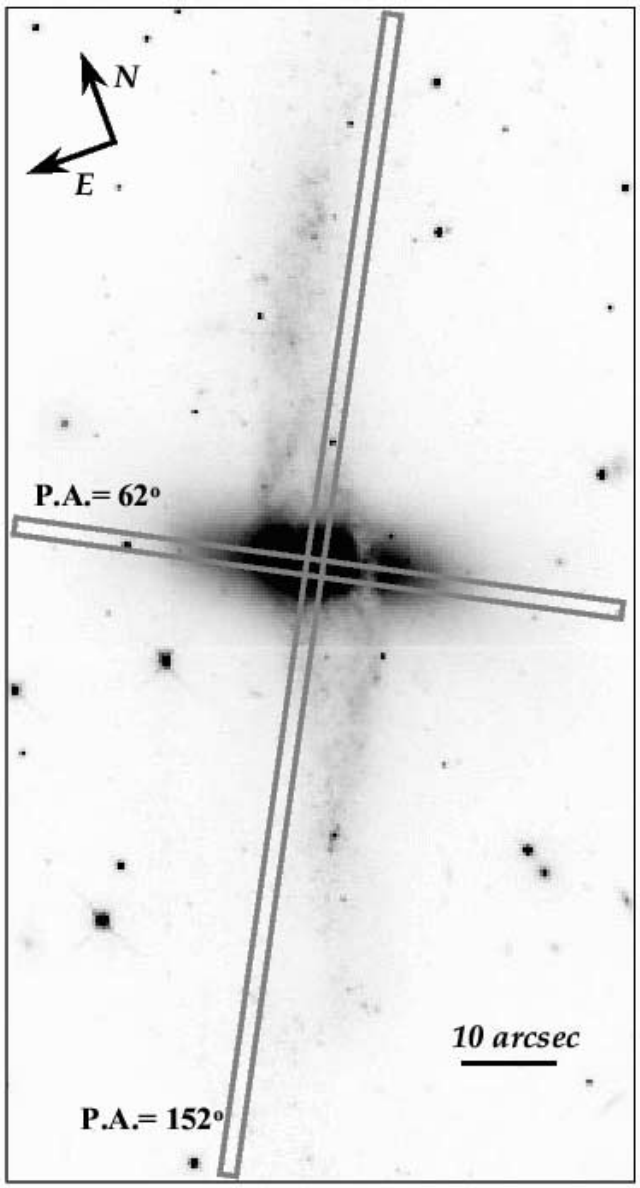

FIG. 1.—*HST I*-band image of NGC 4650A, with the slit positions overlaid.

Combes & Arnaboldi (1996), which differ in the orientation of the main axes and flattening of the dark halo, were both compatible with the observed data. The polar disk luminous mass distribution along the meridian plane may also affect the inner stellar kinematics and induce a triaxial-like perturbation to the axisymmetric stellar mass distribution. Kinematic information along independent position angles on the sky may therefore be required for a reliable mass model. Furthermore, moving to longer wavelengths may help reduce the contamination from the dust (Arnaboldi et al. 1995).

An 8 m class telescope with a spectrograph such as FORS2 (Focal Reducer/Low Dispersion Spectrograph) and a high-efficiency holographic grism in the 1 μm wavelength range would allow us to study the stellar motions of the NGC 4650A inner spheroid, via the absorption-line spectroscopy of the calcium triplet (CaT) lines, at 8498, 8542, and 8662 Å. These lines are the strongest features in the stellar continuum for a large variety of stellar types (Cenarro et al. 2001). In this work, we present our measurements for the radial velocity, the velocity dispersion profile, and the Gauss-Hermite parameters H_3 and H_4 along the main photometric axes of the central spheroid in NGC 4650A. We then discuss their implication on the proposed mass models and formation scenario for PRGs. In what follows, we adopt 2905 km s^{-1} as the heliocentric systemic velocity of NGC 4650A (Arnaboldi et al. 1997) and $H_0 = 70$ km s^{-1} Mpc^{-1}, which implies $1'' = 201$ pc.

2. OBSERVATIONS AND DATA REDUCTION

The spectra were obtained with FORS2 at UT4, on the European Southern Observatory (ESO) Very Large Telescope (VLT), in service mode, during observing run 70.B-0277. FORS2 was equipped with the MIT CCD 910, with an angular resolution of 0.″125 pixel^{-1} and a binning of 2 pixels, so the final scale is 0.″25 pixel^{-1}. Spectroscopic observations were carried out with a slit 1.″6 wide and 6.′8 long and grism GRIS 1028z+29 in the 7730–9480 Å wavelength range, which covers the redshifted absorption lines of the CaT at the systemic velocity of NGC 4650A. The nominal spectral resolution is 0.86 Å pixel^{-1}. Spectra were acquired at the position angles of the photometric major (P.A. = 62°) and minor (P.A. = 152°) axes (Iodice et al. 2002) of the stellar spheroid (Fig. 1). A total integration time of 5 hr was acquired for the major axis and 4.5 hr for the minor axis, with an average seeing of 0.″9 and 0.″83, respectively. In the final median-averaged spectra we reach a limiting surface brightness of $\mu_I =$ 23 mag arcsec^{-2} at $r = 20.''5$ along the spheroid major axis. Spectra of standard template stars of the K0 III and K3 III spectral types were also acquired and trailed along the slit.

The frames were bias-subtracted, flat-fielded, and calibrated using standard IRAF tasks, with helium, argon, and neon arc lamps taken for each observing night. The final solution for the wavelength calibration reaches an rms of 0.07 Å. The instrumental resolution measured from the arc lamp spectra is $\sigma = 2.1$ Å; at the CaT wavelengths, this is equivalent to a velocity resolution of $\sigma = 70$ km s^{-1}.

The sky spectrum was extracted at the outer edges of the slit, where there is no galaxy light, and subtracted off each row of the two-dimensional spectra by using the IRAF task `background` in the TWODSPEC.LONGSLIT package. On average, a sky subtraction better than 1% was achieved; in the region for $\lambda \geq 8740$ Å, where the sky emission lines are stronger and blended (Fig. 2), residuals are less than 2%. After sky subtraction, for each P.A. the scientific frames were co-added to a final median-averaged two-dimensional spectrum. The final spectrum from the major-axis slit at the center of NGC 4650A is shown in Figure 2.

The final steps of the data processing were (1) the binning of the spectra along the spatial direction to achieve a minimum signal-to-noise ratio (S/N) of $\geq$50 at all radii (which is the S/N measured at the last data points, while the central pixels have higher S/N by up to a factor of 4) and to leave no more than two independent data points within the seeing disk and (2) removal of the galaxy continuum by fitting a forth-order polynomial (for a detailed description of the procedures, see Bender et al. 1994).

3. NEW KINEMATICS OF THE CENTRAL SPHEROID: SYSTEMATICS AND ERROR ESTIMATE

The line-of-sight velocity distribution (LOSVD) was recovered from the continuum-removed spectra using the Fourier correlation quotient (FCQ) method (Bender 1990; Bender et al. 1994). By assuming that the LOSVD is described by a Gaussian plus third- and fourth-order Gauss-Hermite functions (van der Marel & Franx 1993; Gerhard 1993), the rotational velocities v, velocity dispersions σ, and first-order deviations from Gaussian profiles H_3 and H_4 were derived at each radius. The best fit to the

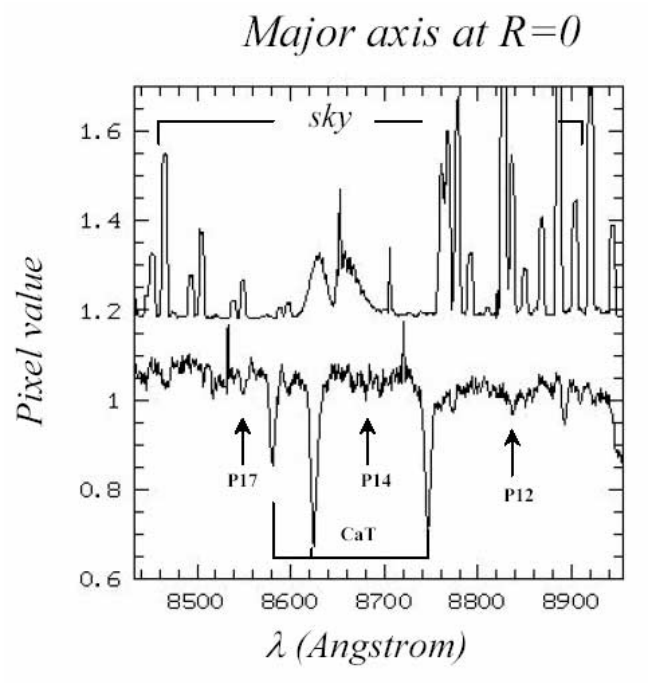

FIG. 2.—Normalized spectra along the major axis in the center of the spheroid (*bottom*), where CaT and PaT lines are marked, and along the sky. Note that the emission lines in the sky are stronger for $\lambda \geq 8740$ Å, where the Paschen line Pa12 is located.

spheroid spectrum was obtained with the K3 III template, while the K0 III stellar template was discarded because of a significant mismatch.

Both statistical and systematic errors for our radial velocity, σ, and the H_3 and H_4 parameters were studied via Monte Carlo simulations (Bender et al. 1994; Mehlert et al. 2000). It turns out that for all these kinematic quantities, the statistical errors dominate with respect to systematic errors at all radii.

3.1. *Influence of Paschen Lines*

The three lines of the Paschen sequence (PaT), Pa13, Pa15, and Pa16, at $\lambda_{\rm rest} = 8665$, 8545, and 8502 Å, lie within the red wings of the CaT lines (Cenarro et al. 2001). They could affect the measured values of v and σ if the adopted stellar template does not match them. Therefore, we need to quantify the equivalent width of the Paschen hydrogen lines and their strength along the slit and compare them with the features in the stellar template spectrum before we derive the spheroid stellar kinematics in NGC 4650A.

We measured the equivalent width (EW) of the unblended Paschen lines Pa14 and Pa17, hereafter Pa(17-14), at $\lambda_{\rm rest} =$ 8598 and 8467 Å and of Ca II at $\lambda_{\rm rest} = 8498$ and 8542 Å along the slit for the two axes; the EW of the Paschen absorption line Pa12 ($\lambda_{\rm rest} = 8750$ Å) cannot be measured reliably because of some strong sky lines' residuals that affect the estimates of the continuum flux (Fig. 2).

In Figure 3, we show the Pa(17-14) and the Ca II EWs and their ratios along the two axes. In the central region of the NGC 4650A spheroid and along its major axis, the Pa(17-14) and the Ca II EWs are similar to those computed for a synthetic galaxy spectrum using the K3 III template star. They are consistent with the values of EWs observed for the stellar integrated light of early-type galaxies (Saglia et al. 2002; Falcón-Barroso et al. 2003).

Along the minor axis, at distances larger than 5″, the Pa(17-14) versus Ca II EW ratio seems to reach values that are comparable to those observed for star-forming galaxies (Saglia et al. 2002). The larger values for the Pa(17-14) EW at these radii may indicate a contribution to the light from young stars in the polar disk.

In order to test whether the contribution of a young stellar population may affect the kinematics, we produced synthetic spectra combining stars of spectral types A and K and measured the Pa(17-14) versus Ca II EW ratio. Figure 3 shows that a template with an increasing contribution from an A-type spectrum, from a 20%(A) + 80%(K) to a 50%(A) + 50%(K), has Pa(17-14) EWs that match the larger values measured in the outer regions of the spheroid minor axis. Once this synthetic spectrum is broadened to 80 km s^{-1} dispersion and analyzed using a pure K template with the FCQ method, the measured velocity dispersion is then 86, 90, and 100 km s^{-1} for the 20%(A) + 80%(K), 30%(A) + 70%(K), and 50%(A) + 50%(K) cases, respectively.

Along the spheroid minor axis at $4'' < r < 6''$ and $r > 6''$ the Paschen lines' strengths are consistent with those of the 20%(A) + 80%(K) and 50%(A) + 50%(K) templates. From our tests, the effects caused by the contribution from younger stars may cause the measured σ to be overestimated by about 6 and 20 km s^{-1}, respectively.

From the present analysis we can conclude that the K3 III template is adequate for the kinematic analysis in the center and along the major axis. In the outer regions of the minor axis we found that the young stars in the polar disk might cause an increase in the Paschen lines' strength (see also § 4.3). Nonetheless, given the large error bars of the Pa(17-14) EWs, a pure K template is still compatible with the data, and it is adopted to measure the kinematics for both axes and at all radii.

3.2. *Instrumental Resolution*

The kinematics along the major axis of the stellar spheroid in NGC 4650A was previously measured from absorption-line spectra at optical wavelengths (4100–4500 and 5085–5980 Å). The latest measurements based on the Mg b and the Na I absorption lines were performed by Sackett et al. (1994): they reported a central value for the velocity dispersion $\sigma_0 \simeq 60$ km s^{-1}. This is similar to our instrumental spectral resolution, as discussed in § 2, and therefore we must evaluate any possible systematic effects on our measurements.

To this aim, we simulated a synthetic galaxy spectrum using the stellar template spectrum, with different values of the velocity dispersion, from 10 to 200 km s^{-1}, and with S/N in the range 10–120. We then recovered the LOSVD via the FCQ method, using the same template as that adopted for our analysis. We found that for S/N $\geq$ 50 and an input velocity dispersion larger than 50 km s^{-1}, the systematic error is less than 10 km s^{-1}; for $\sigma < 50$ km s^{-1}, the measured values tend to the asymptotic value of 40 km s^{-1}. For smaller values of S/N, the systematic errors are larger. Based on these results, we have adopted a variable spatial binning along the slit that increases with distance from the galaxy center so that S/N $\geq$ 50 is achieved as we step to larger distances from the NGC 4650A center. At the galaxy center, S/N $\sim$ 200.

4. LOSVD ALONG THE PRINCIPAL PHOTOMETRIC AXES OF NGC 4650A

Quantitative photometry of NGC 4650A has shown that the internal structure of this object is rather complex (Gallagher et al. 2002; Iodice et al. 2002), and we now wish to examine the correlation between morphological subcomponents and kinematic signatures. In Figures 1 and 4 we overlay the slit positions on the *Hubble Space Telescope* (*HST*) images of NGC 4650A, and in

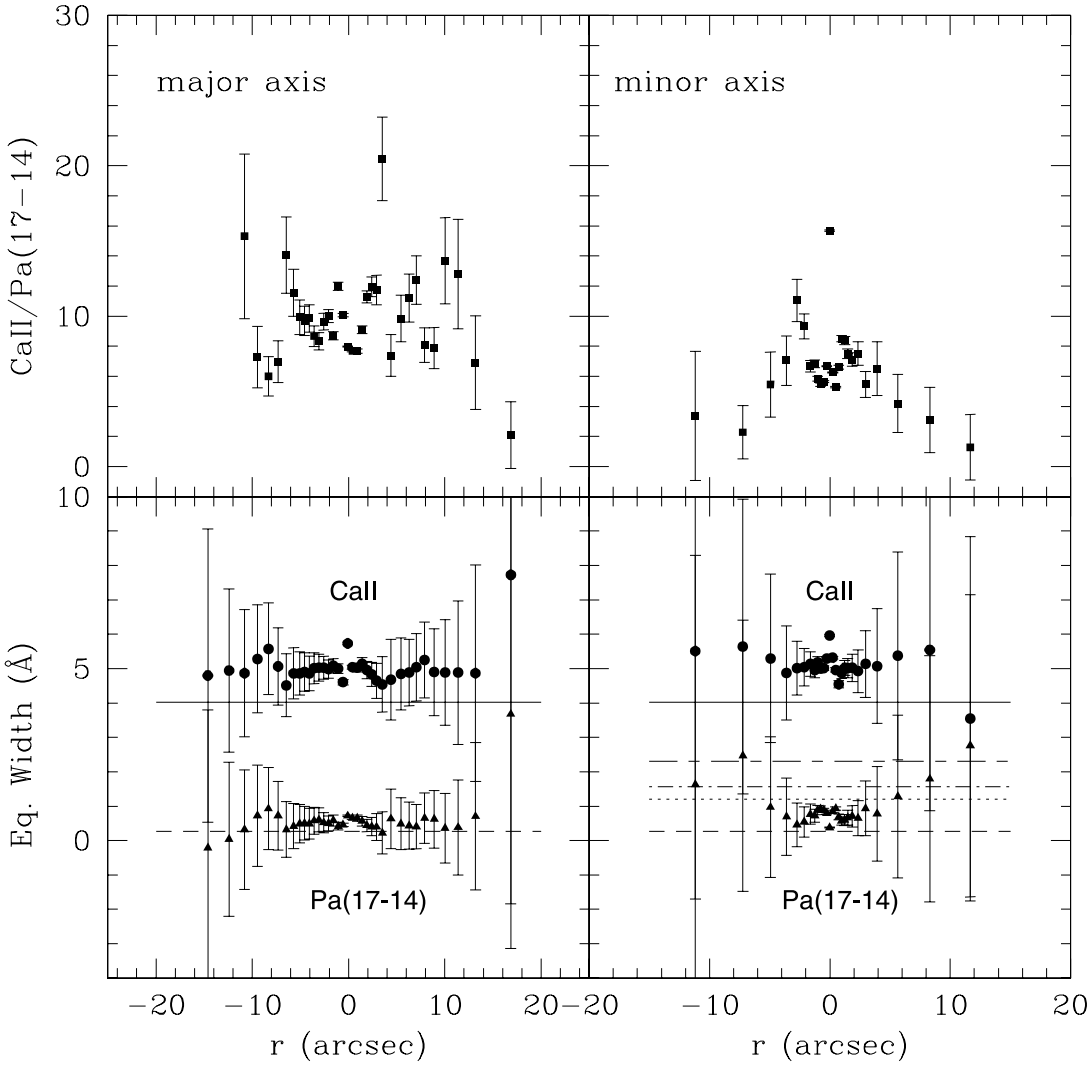

FIG. 3.—*Top:* EW ratio between the Ca II and Pa(17-14) lines vs. distance from the galaxy center along the major (*left*) and minor (*right*) axis. *Bottom:* EW of the Ca II lines (*circles*) and Pa(17-14) lines (*triangles*) along the major (*left*) and minor (*right*) axis. Solid and dotted lines indicate the Ca II and Pa(17-14) EW, respectively, in the synthetic galaxy spectrum made by a pure K star template. In bottom right panel, the Pa(17-14) EWs for different synthetic spectra are also shown. Synthetic spectra were obtained by combining stars of spectral types A and K (see also § 3.1): then dotted line is for 20%(A) + 80%(K), the dash-dotted line is for 30%(A) + 70%(K), and the short-dash–long-dashed line is for 50%(A) + 50%(K).

the following section we briefly describe the luminous subcomponents along both axes, which affect the stellar light in the spectra. In Figures 5 and 6 we plot the rotation curve, velocity dispersion, and the H_3 and H_4 profiles for both the major and minor axes of the spheroid in NGC 4650A.

4.1. *Morphological Components along the Main Axes*

Along the major axis (P.A. = 62°), the central spheroid extends to $r_{\rm outer} = 25''$ from the center in the *I* band, and $r_{\rm outer}$ is about $4r_e$; the equivalent effective radius for the central spheroid in NGC 4650A is $r_e = 6''.7$ and is evaluated by fitting the whole *I*-band light profiles with a Sersic law $I(r) \propto r^{1/n}$, where $n \sim 2$. The dust associated with the polar disk, whose absorption is seen in front of the central spheroid on the southwest side (Fig. 1), affects the light profile along the major axis at $r \sim 5''$; it is also seen in the extracted light profile along the slit (Fig. 4, *right*). For $r < 5''$, Iodice et al. (2002) showed that the polar disk and the spheroid light coexist (Fig. 4, *top left*); within $r < 1''$ there is a very luminous, compact nucleus, of about 20 pc ($\sim 0''.1$) in radius and $L_I \sim 8 \times 10^7\ L_\odot$, which is superimposed on a more extended and rounder structure, of about 60 pc $\sim 0''.3$ (Gallagher et al. 2002).

Along the minor axis (P.A. = 152°), the light from the polar disk is present at all radii and at $r > 6''$ from the center becomes dominant over the spheroid light. The residual image (by Iodice et al. 2002) shows that on the southeast side of the center the spectrum will include more light from polar-disk–related features than on the northwest side. Within $r < 1''$, the minor-axis light is dominated by the luminous compact nucleus.

4.2. *The Major-Axis Kinematics*

The rotation curve is measured out to $20''.5$ ($\sim$4 kpc), i.e., about $3r_e$ (Fig. 5), which corresponds to a surface brightness of $\sim$23 mag arcsec^{-2} in the *I* band. At $16''$ ($\sim$3 kpc) from the center, the velocity increases; it reaches the maximum value of nearly 100 km s^{-1} on the northeast side and slightly lower, $\sim$70 km s^{-1}, on the southwest side. The rotation curve is not symmetric: at $1'' < r < 5''$ southwest (i.e., from 200 pc to 1 kpc), the rotation curve shows lower velocities than the corresponding northeast side. This was already noticed by Sackett et al. (1994), and a possible cause is the light contribution from the stars in the polar disk, which passes in front of the spheroid on this side, as we discuss in detail in § 4.1.

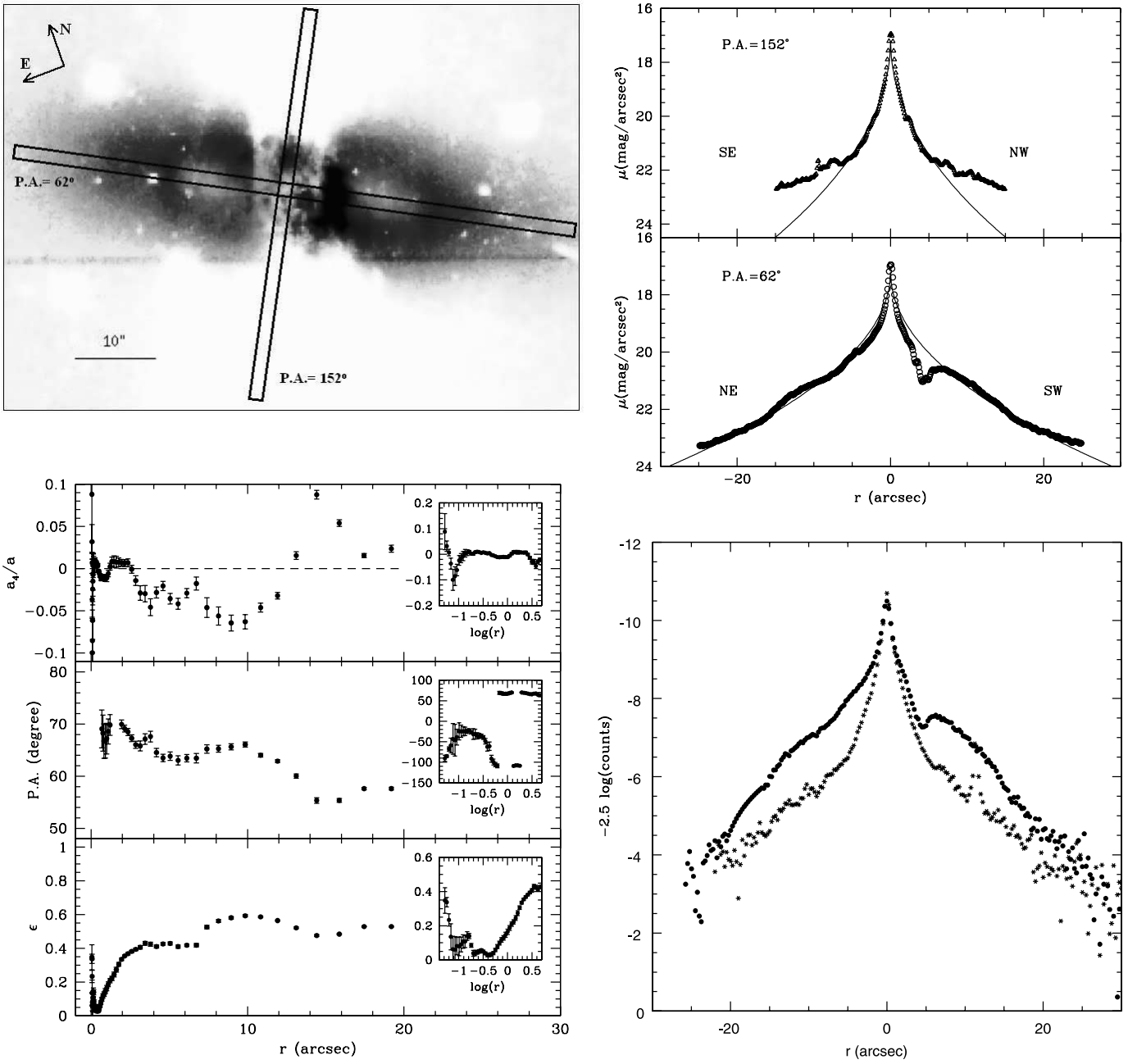

FIG. 4.—*Top left:* Residual image, obtained as the ratio between the whole galaxy frame and the two-dimensional model of the spheroid light distribution in the *I* band (see Iodice et al. 2002 for details). Units are intensity; lighter colors correspond to those regions where the galaxy is brighter than the model, while darker colors correspond to those regions where the galaxy is fainter than the model. *Top right:* Surface brightness profiles (*open circles*) and $r^{1/n}$ fit (*solid line*) along the major and minor axes of the inner stellar spheroid (from Iodice et al. 2002). *Bottom left:* Ellipticity, P.A. profiles, and isophotal shape parameter a_4 of the stellar spheroid in the *I* band. *Bottom right:* Uncalibrated luminosity profiles extracted through the slit along the major (*circles*) and minor (*asterisks*) axes.

In the nuclear regions (Fig. 5, *bottom*), within a 0.″5 radius from the center, the sense of rotation is reversed, and the measured velocity dispersion decreases to ∼69 km s^{-1}. These kinematic features correlate with the presence of the bright compact nucleus and the photometric properties, as for example the variation of P.A. and ellipticity profiles with respect to larger radii (Fig. 4). Outside the nuclear region, the velocity dispersion profile is flat, $\sigma \sim 74$ km s^{-1}, out to at least 14″ (∼3 kpc).

The H_3 profile is almost constant and is consistent with zero within the error bars, from the center out to about 6″; its value tends to increase for larger radii. The H_4 profile is zero at the center and then become slightly negative, with an almost constant value of −0.05 on the southwest side and a value between −0.05 and −0.1 out to 16″ (∼3.2 kpc) on the northeast side.

4.3. *The Minor-Axis Kinematics*

On the minor axis, the kinematics can be measured out to 12″–15″ from the center (Fig. 6, *top*). The central spheroid dominates the stellar light for $r \leq 6''$ ($\sim r_e$), and while the polar disk structure is present at all radii, its surface brightness dominates the light at $r > 6''$.

At $r < 4''$, small wiggles with $|v| \simeq 10$ km s^{-1} are visible, but the v profile is generally consistent with no rotation. At $r > 4''$ the rotation becomes significant and reaches $v_{\max} \simeq 40$ km s^{-1} at 10″, with slightly larger LOS velocities on the southeast.

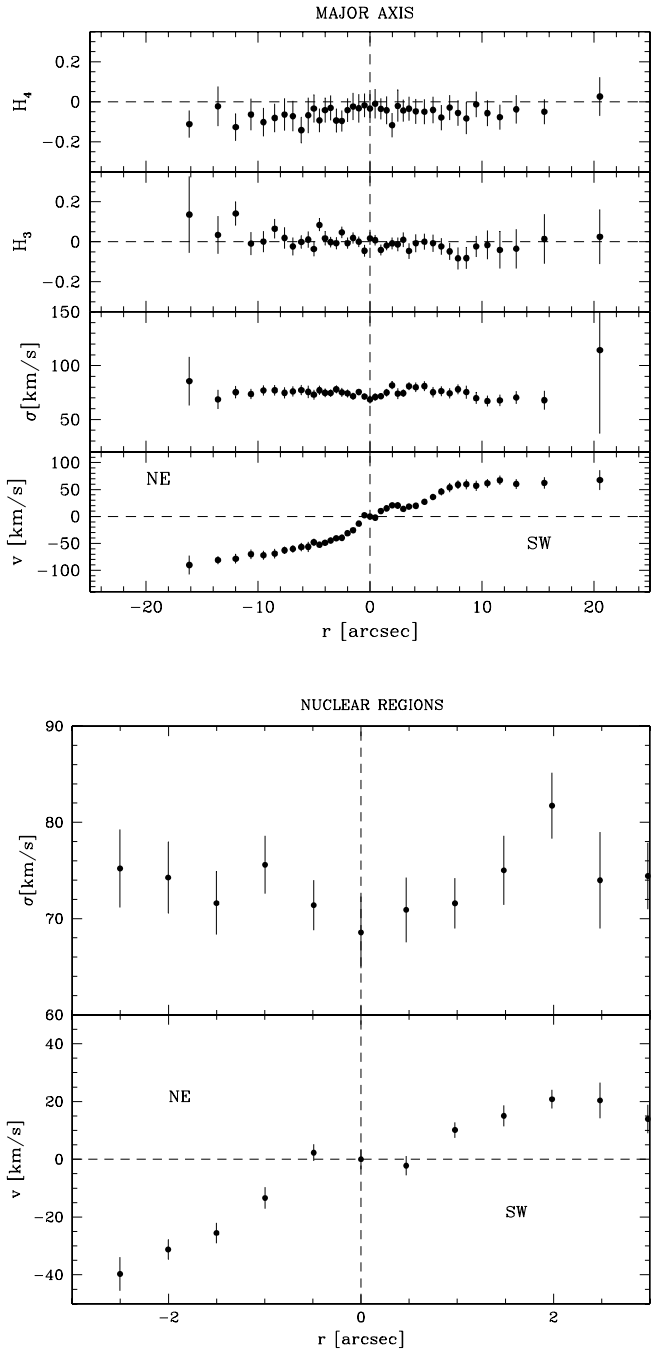

FIG. 5.—*Top:* Rotation curve (v), velocity dispersion (σ), H_3, and H_4 derived for the major axis, P.A. = 62°, of the inner spheroid in NGC 4650A. *Bottom:* Rotation curve (v) and velocity dispersion (σ) in the nuclear regions of the stellar spheroid.

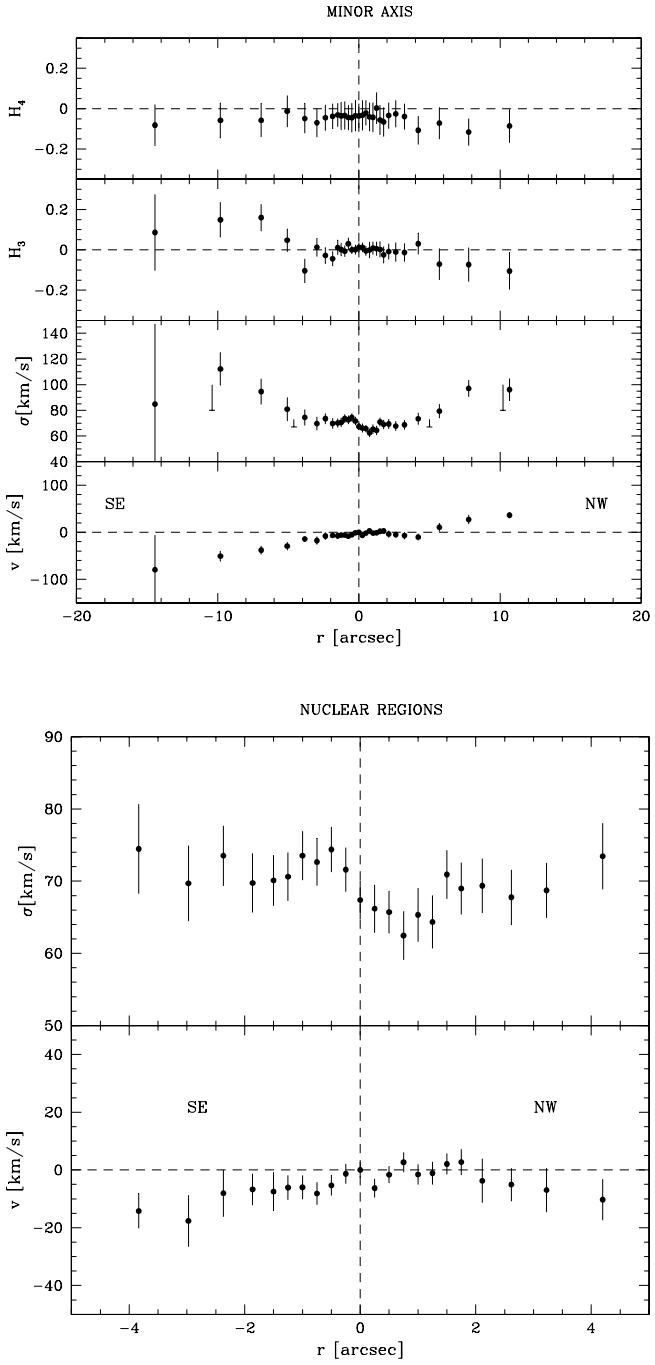

FIG. 6.—*Top:* Rotation curve (v), velocity dispersion (σ), H_3, and H_4 derived for the minor axis, P.A. = 152°, of the stellar spheroid. The downward error bars at $r = \pm 5''$ and $\pm 10''$ show the systematic effect on the measured σ-values caused by a young population of stars contributing up to 20%–50% of the total light (see § 3.1 for details). *Bottom:* Rotation curve (v) and velocity dispersion (σ) in the nuclear regions of the spheroid in NGC 4650A.

The measured velocity dispersion is about $\simeq$70 km s^{-1} in the central parts and then increases to $\simeq$100 km s^{-1} at $r = 10''$. For $r < 2''$ ($\sim$0.4 kpc), the velocity dispersion profile is asymmetric with respect the galaxy center (see the nuclear region enlargement in Fig. 6, *bottom*); larger σ-values ($\sim$68–74 km s^{-1}) are measured on the southeast than on the northwest side ($\sigma \sim 62$–68 km s^{-1}).

At $r < 4''$ ($\sim$0.8 kpc), where the velocity is nearly zero, the H_3 and H_4 profiles are roughly constant, at values equal to 0.0 and -0.05, respectively. At $r > 4''$, where v and σ increase, the H_3 profile also changes and becomes positive on the southeast and negative on the northwest. The measured H_4 profile becomes slightly more negative (~ -0.1) at these radii. As discussed in § 3.1, the presence of young stars in the polar disk may partially account for the measured increase in the velocity dispersion profile along the minor axis. Once we consider these systematic effects on σ due to an increase of the Paschen EWs (§ 3.1), the minor-axis measurements are consistent with a flat or slightly rising velocity dispersion profile for $r > 4''$ (Fig. 6). This interpretation may still not be unique: the coherent variation

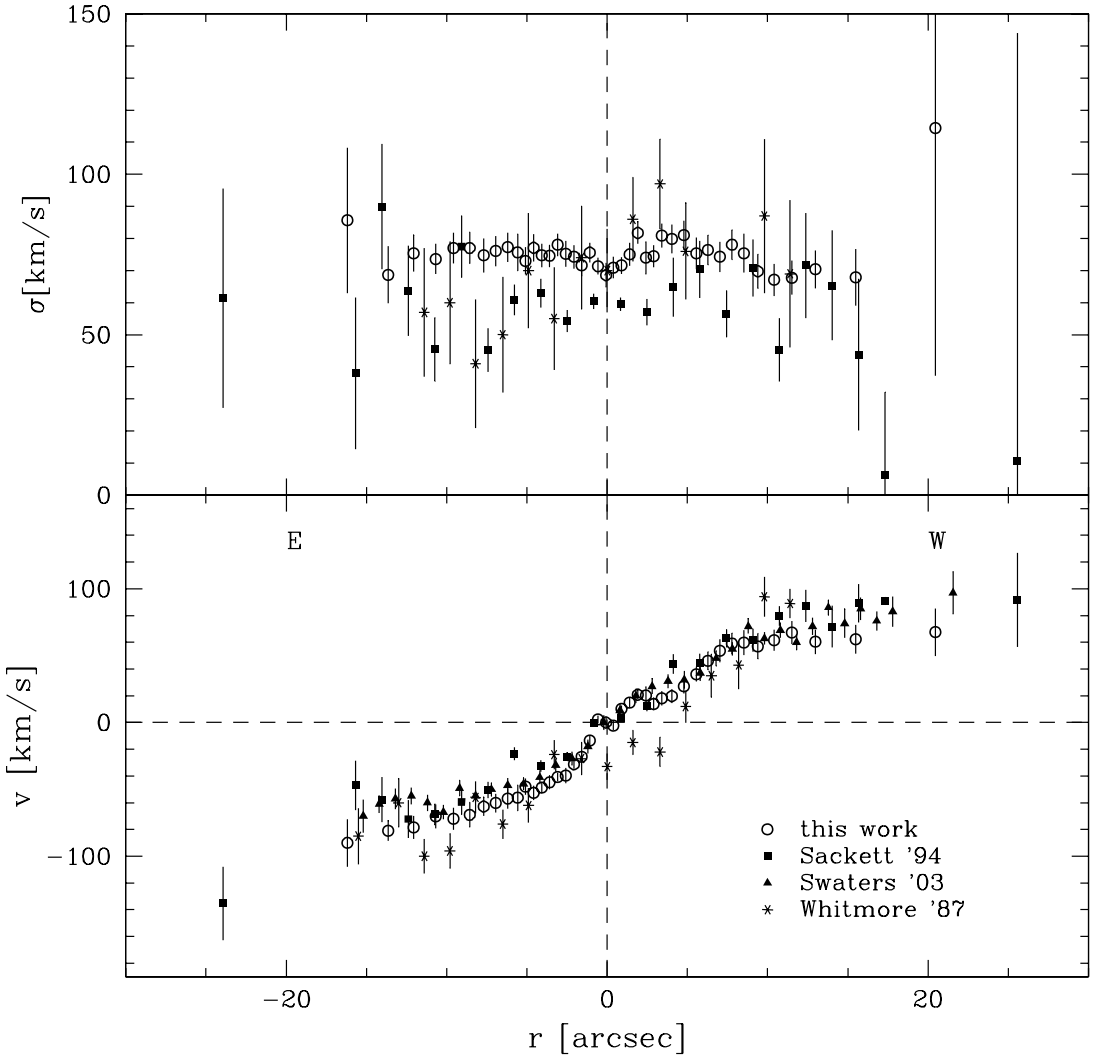

FIG. 7.—Rotation curve and velocity dispersion profile along the major axis of the stellar spheroid obtained in this work compared with those in the literature by Whitmore et al. (1987; P.A. = 63°), Sackett et al. (1994; P.A. = 61°), and Swaters & Rubin (2003; P.A. = 63°). [*See the electronic edition of the Journal for a color version of this figure.*]

observed in the v, σ, H_3, and H_4 profiles for $r > 4''$ may also be related to the spheroid structure.

5. DISCUSSIONS AND CONCLUSIONS

We have obtained new high angular resolution, high signal-to-noise ratio spectra along the photometric axes of the stellar spheroid in NGC 4650A. Compared to previous kinematics studies, the new observations show (1) a kinematic signature of a decoupled core and (2) a nonzero rotational velocity and an increasing velocity dispersion along the minor axis. In the following we discuss them and address the main conclusions about the structure and formation of NGC 4650A.

5.1. *Comparison with Previous Observations and Dynamical Models*

We now compare the current rotation velocities and velocity dispersion measurements with those previously published in the literature (Whitmore et al. 1987; Sackett et al. 1994; Swaters & Rubin 2003). Our data represent a significant improvement in angular resolution, which is needed for the understanding of the nuclear regions, and no velocity dispersion measurements were available for the spheroid minor axis prior to this work. The rotation curve along the polar disk at P.A. = 158° was measured from the Hα emission line (Whitmore et al. 1987) and from optical absorption lines at P.A. = 155° (Swaters & Rubin 2003), with slits aligned separately along north and south parts of the polar disk and thus not through the center of the spheroid; both were obtained at a slightly different P.A. from that of the minor-axis spheroid (P.A. = 152°; Iodice et al. 2002).

A direct comparison of the major-axis kinematics data, v and σ, is shown in Figure 7; previously published data show a larger scatter for the velocity dispersion measurements, while the agreement is good for the rotation curves. Our kinematic data are consistent within the errors: the new rotation curve is in good agreement with the previous ones, and our σ profile has clearly benefited from a substantial increase in S/N, thanks to the collecting area of an 8 m telescope. The new σ measurements are in agreement with those by Whitmore et al. (1987), while they are systematically larger than the measurements from Sackett et al. (1994). The average difference in this case is about 15 km s^{-1}, similar to the 19 km s^{-1} that Sackett et al. (1994) subtracted off the data to account for their systematics.

The new high-resolution CaT spectra are better tracers of the kinematics for the NGC 4650A spheroid than those previously

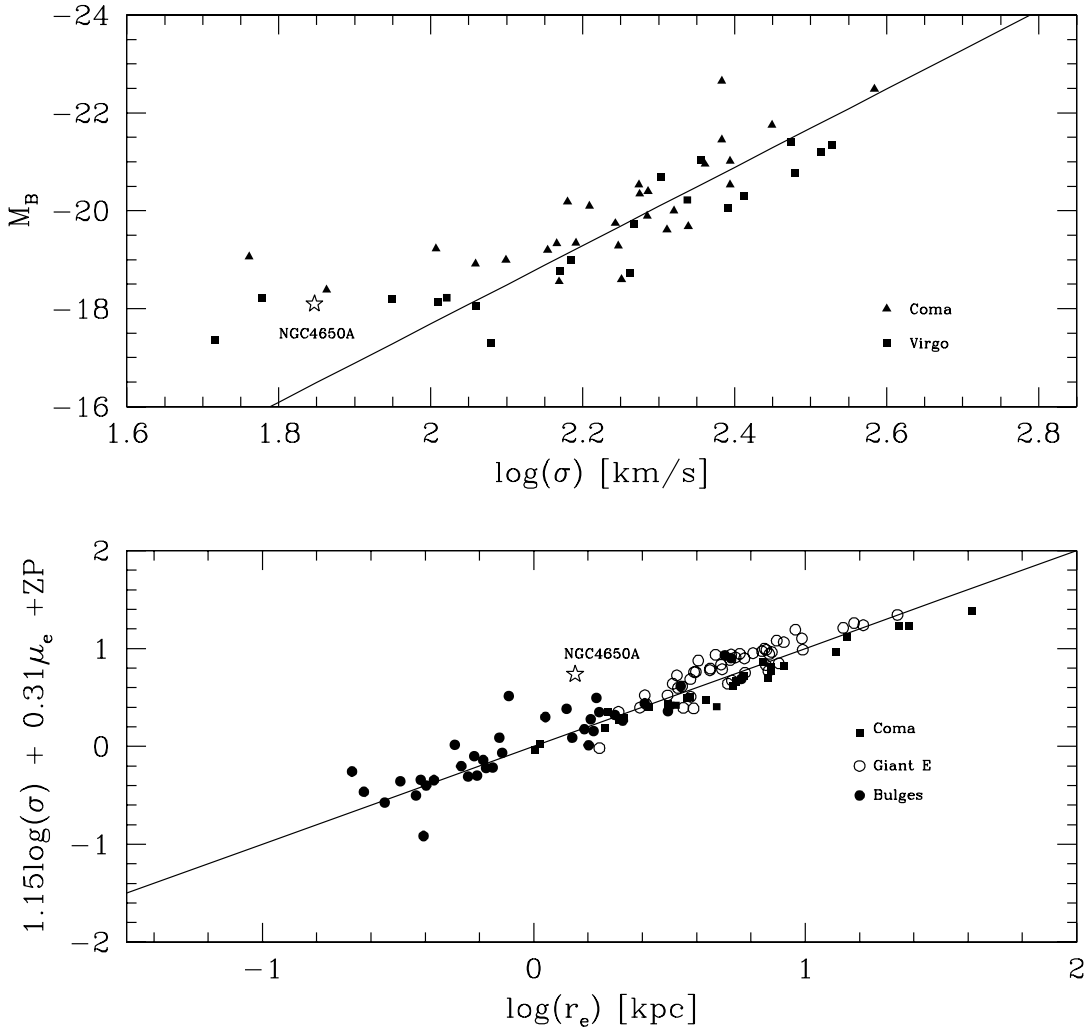

FIG. 8.—*Top:* Faber-Jackson relation between the central velocity dispersion and the absolute *B* magnitude. Local early-type galaxies in the Virgo Cluster (*squares*) and Coma Cluster (*triangles*) are from Dressler et al. (1987); the straight line is the principal components fit of these data by Ziegler & Bender (1997). The position of the spheroid in NGC 4650A is shown on the figure. *Bottom: B*-band FP for different morphological types of galaxies: early-type galaxies in the Coma Cluster are from Jorgensen et al. (1996), giant elliptical galaxies are from Bender et al. (1992), and bulges of disk galaxies are from both Falcón-Barroso et al. (2002) and Bender et al. (1992). The straight line is the fit performed by Falcón-Barroso et al. (2002), which includes both Coma galaxies and bulges. The position of the stellar spheroid in NGC 4650A is shown on the figure.

available. The higher angular resolution and the net increase in S/N allow us to (1) measure a *flat* velocity dispersion profile along the spheroid major axis, while previous σ measurements were too scattered to reliably establish any trend with radius, (2) detect a decrease of the velocity dispersion in the center, and (3) detect a hint of increasing σ in the northeast, as previously noticed by Sackett et al. (1994).

The measured flat velocity dispersion profile along the spheroid major axis shows that neither the linear decreasing fit $\sigma_r(r) = \sigma_r(0) - Kr_d$ proposed by Sackett et al. (1994) nor the exponential empirical law $\sigma_r(r) = \sigma_r(0) \exp\,[-(r/4r_d)^4]$ proposed by Combes & Arnaboldi (1996) reproduces the observed trend with radius. Previous conclusions that the same authors drew were based on data that are no longer valid, and the dynamical model for NGC 4650A must be revised.

5.2. *The Spheroid Kinematics*

The stellar spheroid $v/\sigma - \epsilon$ relation.—The light distribution of the central stellar spheroid in NGC 4650A is fit by a nearly exponential surface brightness profile, with $r_e = 6\farcs7$ and $\epsilon = 0.46$ in the *I* band, and is nearly edge-on as inferred from the presence of a thin disk aligned with the spheroid's major axis (Iodice et al. 2002). This is a low-luminosity spheroid, with $M_B \sim -18.1$ (Gallagher et al. 2002) based on *HST* photometry.

The observed kinematics along the major axis is consistent with that of a spheroidal galaxy supported by rotation: at $r \geq 2r_e$, where the ellipticity $\epsilon \sim 0.5$, we estimate $(v/\sigma)^* \sim 0.96$. The anisotropy parameter $(v/\sigma)^*$ is defined as the ratio of the observed value of (v/σ) and the theoretical value for an isotropic oblate rotator $(v/\sigma)_{\rm oblate} = [\epsilon/(1-\epsilon)^{1/2}]$ (Binney 1978). For a total *B* magnitude of $M_B \sim -18.1$ (Gallagher et al. 2002), in the plane $\log\,(v/\sigma)^* - M_B$ the central spheroid of NGC 4650A is located in the region of low-luminosity elliptical galaxies flattened by rotation (see Fig. 18 in Bender et al. 1994).

Faber-Jackson relation and the fundamental plane.—We have investigated the position of the stellar spheroid in NGC 4650A with respect to the Faber-Jackson relation (FJR; Faber & Jackson 1976) and fundamental plane (FP; Djorgovski & Davis 1987) of elliptical galaxies. In Figure 8 (*top*) we compare the absolute *B* magnitude and the central velocity dispersion for the spheroid in NGC 4650A with those for elliptical galaxies in the Virgo and Coma Clusters (in the sample studied by Dressler et al.

1987). For the observed velocity dispersion, the spheroidal component in NGC 4650A is more luminous with respect to the predicted value by the best fit of the FJR (which did not include the five galaxies with $\log \sigma < 2$).

With respect to the B-band[12] FP of elliptical galaxies and bulges (by Bender et al. 1992; Jorgensen et al. 1996; Falcón-Barroso et al. 2002), the spheroid in NGC 4650A falls slightly above the average relation for Es and S0 in the Coma Cluster (see Fig. 8, *bottom*). Forbes & Ponman (1999) showed that bluer early-type galaxies have larger deviations from the FJR: the observed deviations of the NGC 4650A spheroid from both the FJR and the FP, toward higher luminosity, are consistent with the stellar component being younger and bluer (Gallagher et al. 2002; Iodice et al. 2002) than that in standard early-type galaxies.

Kinematics on the spheroid minor axis.—The new kinematics observed along the minor axis is rather complex and needs to be discussed in some detail. In the inner regions ($r \leq 4''$–$6''$), where the spheroid's light dominates, the observed kinematics is consistent with an isotropic oblate spheroid, as suggested by the major-axis kinematics. The LOS velocities are close to zero, and the velocity dispersion measurements are very similar to the constant values measured along the major-axis slit. Within these regions, the slightly asymmetric circular velocity and dispersion profiles, with respect to the galaxy center, may reflect the contamination by the "inner polar disk arms" (Fig. 4). On the southeast side with respect to the galaxy center, along the minor-axis slit, the light includes most of the inner polar disk arms (Gallagher et al. 2002; Iodice et al. 2002), and both the LOS velocity and the velocity dispersion at $r \geq 0\farcs5$ are larger than those observed on the northwest side (Fig. 6).

At larger radii (for $r \geq 6''$), the dispersion increases and larger rotational velocities are observed. Three possible interpretations are currently viable: (1) the observed profiles are tracing the intrinsic spheroid kinematics or (2) these effects are produced by contamination of the stellar motion in the polar disk or (3) by stronger Paschen lines in a mixed population (§ 3.1).

If the stellar spheroid has indeed intrinsic minor-axis rotation (Fig. 6, with $\mu \sim 0.23$ at $r \sim 0.5 r_e$),[13] and the presence of isophotal twist (Fig. 4), both suggest that the system could be triaxial (Wagner et al. 1988; Franx et al. 1991). If the flat or slightly increasing velocity dispersion profile at large radii is intrinsic, it may trace the presence of larger masses along the meridian plane. This would be consistent with the presence of a massive polar disk (Arnaboldi et al. 1997; Iodice et al. 2002) and with the empirical evidence for a dark halo flattened along this direction from the Tully-Fisher relation of PRGs (Iodice et al. 2003). The potential generated by a bar can also induce minor-axis rotation (Athanassoula 1992), but the presence of a bar in the stellar spheroid of NGC 4650A is not supported by the photometry.

5.3. *The Nuclear Regions of NGC 4650A*

The stellar spheroid of NGC 4650A is known to contain a very luminous, compact nucleus, whose extension is about 20 pc ($\sim 0\farcs1$) and whose luminosity is $L_I \sim 8 \times 10^7\ L_\odot$, which is superimposed on a more extended and rounder structure, of about 60 pc (Gallagher et al. 2002; see also § 4). The high angular resolution of our spectra allows us to reveal the kinematic signature of the nucleus: within a $0\farcs5$ radius along the major axis, we observe a decoupled component in the circular velocity profile, associated with a lower velocity dispersion. Such features indicate the presence of a small core, kinematically distinct from the main central spheroid, whose extension ($\sim$100 pc) is consistent with the photometry. This is also comparable with the sizes of the kinematically decoupled cores (KDCs) observed in "normal" early-type galaxies, which vary from hundreds of kiloparsecs (Kropolin & Zeilinger 2000) to about 30–60 pc for the very small cores detected in *HST* images (Krajnović & Jaffe 2004). The *HST* data for KDCs in early-type galaxies show that the isophotes in these regions are rounder and have a different P.A. with respect to the outer regions (Krajnović & Jaffe 2004): this behavior is very similar to what is observed in the central $0\farcs5$ radius in NGC 4650A (Fig. 4).

The observed KDC kinematics in early-type galaxies has very similar features to those measured in the nuclear regions of NGC 4650A. On the whole, the velocity profile is characterized by a central asymmetry, with a flat or a decreasing velocity dispersion profile at the corresponding nuclear radii.

An upper limit to the mass of the KDC observed in NGC 4650A is $\sim 10^8\ M_\odot$: here we have assumed that the circular-orbit speed at $0\farcs5$ from the center is less than the squared sum of the velocity dispersion and the measured circular velocity. The nuclear mass estimate for NGC 4650A is higher than the masses of the star cluster nuclei derived for late-type spiral galaxies, which vary from 10^5 to $10^7\ M_\odot$ (Matthews & Gallagher 2002; Böker et al. 2001). As already suggested by Gallagher et al. (2002), this is consistent with a more luminous star cluster nucleus in NGC 4650A, for which we estimate a mass-to-light ratio $M/L \sim 1.5\ M_\odot/L_\odot$. The moderate age for the star cluster nucleus in NGC 4650A (Gallagher et al. 2002), based on the $B - I$ color, is consistent with the absence of Paschen lines in the nuclear regions (§ 3.1).

KDCs are often related to a secondary event in a galaxy evolution (Bertola & Corsini 1999). Numerical simulations indicate that kinematically peculiar nuclei may result from the merging of two disk galaxies, where the size of the KDC becomes smaller (less than the effective radius) as the mass ratio of the two merging galaxies becomes smaller than 1 (Balcells & Gonzalez 1998). KDCs are also present in barred galaxies and are characterized by a low velocity dispersion in the center (Emsellem et al. 2001). In this case, they are the result of a secular evolution, rather than of an interaction, because the gravitational torque by the bar drives the gas toward the central regions, which then forms new stars with lower velocity dispersion (Wozniak et al. 2003), but in NGC 4650A, no evidence for a barlike structure was detected (Gallagher et al. 2002; Iodice et al. 2002), and the ellipticity and P.A. profiles do not show the typical features observed for barred galaxies (Wozniak et al. 1995; Erwin & Sparke 1999).

The formation scenarios for PRGs, either via major merging of two disk galaxies (Bekki 1998a) or accretion of external material (Bournaud & Combes 2003), predict that some gas flows to the galaxy center and quickly forms a small star cluster. This can easily lead to the formation of a KDC in these systems.

5.4. *Implications for the Formation of NGC 4650A*

As discussed in § 5.2, the observed kinematics and the photometry suggest that the central galaxy in NGC 4650A is a spheroid with a nearly exponential surface brightness profile, supported by rotation. In a merging scenario with low relative

[12] The effective radius and the effective surface brightness used to derive the FP for the spheroid in NGC 4650A were estimated by fitting the whole *HST* B-band light profiles with a Sersic law [$I(r) \propto r^{1/n}$], where $n \sim 2$, $\mu_e \sim 23.00 \pm 0.02$, and $r_e \sim 7\farcs1 \pm 0\farcs1$.

[13] According to Binney (1985), the amount of minor-axis rotation is parameterized as $\mu = v_{\rm min}/(v^2_{\rm maj} + v^2_{\rm min})^{1/2}$.

velocity and low impact parameter (Bekki 1998a; Bournaud & Combes 2003), a high mass ratio is required to form a massive polar disk, as observed in NGC 4650A: the "victim" mass should exceed the "intruder" mass. According to simulations of galaxy mergers (e.g., Bournaud et al. 2005) this would convert the intruder into an elliptical-like, not rotationally supported, stellar system. In contrast, in the tidal accretion scenario, with a large relative velocity and a large impact parameter, for a particular orbital configuration and a gas-rich donor, a polar ring and/or disk could form either around a disk or around an elliptical galaxy (Bournaud & Combes 2003). External gas could be also accreted from the cosmic web filaments (Davé et al. 2001; Macciò et al. 2006): in this formation scenario, there are no limits to the mass of the accreted material; thus, a very massive polar disk could develop around either a stellar disk or a spheroid.

The new kinematic data obtained for NGC 4650A suggest that the accretion scenarios are favored; nevertheless, more investigations are needed to solve the discrepancies between the observations and the theoretical predictions.

The authors are very grateful to the referee, V. Rubin, for comments and suggestions that let us improve this work. E. I. wishes to thank E. Cappellaro, F. Patat, and J. Alcalá for their help during data reduction. E. I. is also very grateful to E. M. Corsini, N. R. Napolitano, G. Busarello, and F. La Barbera for many useful discussions and suggestions. We thank R. Swaters for making available the stellar absorption-line rotation curves (derived from the Mg I line in the optical spectrum) for NGC 4650A. E. I. and M. C. acknowledge financial support from the Italian Ministry of Education, University and Research (MIUR) through grant COFIN2004020323. E. I. and M. A. acknowledge financial support from INAF, Project of National Interest (PI: M. A.), and the Swiss National Science Foundation under grant 200020-101766. L. S. S. would like to thank the Max-Planck-Institute for Astrophysics in Garching for their hospitality and the US National Science Foundation for support through grant AST 00-98419. J. S. G. acknowledges financial support by the US National Science Foundation, under grant AST 98-03018, and would also like to thank Basel Observatory for travel support.

REFERENCES

Arnaboldi, M., Freeman, K. C., Sackett, P. D., Sparke, L. S., & Capaccioli, M. 1995, Planet. Space Sci., 43, 1377
Arnaboldi, M., Oosterloo, T., Combes, F., Freeman, K. C., & Koribalski, B. 1997, AJ, 113, 585
Athanassoula, E. 1992, MNRAS, 259, 328
Balcells, M., & Gonzalez, C. G. 1998, ApJ, 505, L109
Barnes, J. E., & Hernquist, L. 1992, ARA&A, 30, 705
Bekki, K. 1998a, ApJ, 499, 635
———. 1998b, ApJ, 502, L133
Bender, R. 1990, A&A, 229, 441
Bender, R., Burstein, D., & Faber, S. M. 1992, ApJ, 399, 462
Bender, R., Saglia, R. P., & Gerhard, O. 1994, MNRAS, 269, 785
Bertola, F., & Corsini, E. 1999, in IAU Symp. 186, Galaxy Interactions at Low and High Redshift, ed. J. E. Barnes & D. B. Sanders (Dordrecht: Kluwer), 149
Binney, J. 1978, MNRAS, 183, 501
———. 1985, MNRAS, 212, 767
Böker, T., van der Marel, R. P., Mazzuca, L., Rix, H.-W., Rudnick, G., Ho, L. C., & Shields, J. C. 2001, AJ, 121, 1473
Bournaud, F., & Combes, F. 2003, A&A, 401, 817
Bournaud, F., Jog, C. J., & Combes, F. 2005, A&A, 437, 69
Cenarro, A. J., Cardiel, N., Gorgas, J., Peletier, R. F., Vazdekis, A., & Prada, F. 2001, MNRAS, 326, 959
Combes, F., & Arnaboldi, M. 1996, A&A, 305, 763
Conselice, C. J., Bershady, M. A., Dickinson, M., & Papovich, C. 2003, AJ, 126, 1183
Davé, R., et al. 2001, ApJ, 552, 473
Djorgovski, S., & Davis, M. 1987, ApJ, 313, 59
Dressler, A., Lynden-Bell, D., Burstein, D., Davies, R. L., Faber, S. M., Terlevich, R., & Wegner, G. 1987, ApJ, 313, 42
Emsellem, E., Greusard, D., Combes, F., Friedli, D., Leon, S., Pecontal, E., & Wozniak, H. 2001, A&A, 368, 52
Erwin, P., & Sparke, L. S. 1999, ApJ, 521, L37
Faber, S. M., & Jackson, R. E. 1976, ApJ, 204, 668
Falcón-Barroso, J., Balcells, M., Peletier, R. F., & Vazdekis, A. 2003, A&A, 405, 455
Falcón-Barroso, J., Peletier, R. F., & Balcells, M. 2002, MNRAS, 335, 741
Forbes, A. D., & Ponman, T. J. 1999, MNRAS, 309, 623
Franx, M., Illingworth, G., & de Zeeuw, T. 1991, ApJ, 383, 112
Gallagher, J. S., Sparke, L. S., Matthews, L. D., Frattare, L. M., English, J., Kinney, A. L., Iodice, E., & Arnaboldi, M. 2002, ApJ, 568, 199
Gerhard, O. 1981, MNRAS, 197, 179
———. 1993, MNRAS, 265, 213
Hibbard, J. E., & Yun, M. S. 1999, ApJ, 522, L93
Iodice, E., Arnaboldi, M., Bournaud, F., Combes, F., Sparke, L. S., van Driel, W., & Capaccioli, M. 2003, ApJ, 585, 730
Iodice, E., Arnaboldi, M., De Lucia, G., Gallagher, J. S., Sparke, L. S., & Freeman, K. C. 2002, AJ, 123, 195
Krajnović, D., & Jaffe, W. 2004, A&A, 428, 877
Kropolin, W., & Zeilinger, W. W. 2000, A&AS, 145, 71
Jorgensen, I., Franx, M., & Kjaergaard, P. 1996, MNRAS, 280, 167
Macciò, A. V., Moore, B., & Stadel, J. 2006, ApJ, 636, L25
Matthews, L. D., & Gallagher, K. 2002, ApJS, 141, 429
Mehlert, D., Saglia, R., Bender, R., & Wegner, G. 2000, A&AS, 141, 449
Naab, T., & Burkert, A. 2003, ApJ, 597, 893
Sackett, P. D., Rix, H., Jarvis, B. J., & Freeman, K. C. 1994, ApJ, 436, 629
Sackett, P. D., & Sparke, L. S. 1990, ApJ, 361, 408
Saglia, R., Maraston, C., Thomas, D., & Bender, R. 2002, ApJ, 579, L13
Schweizer, F. 1999, in IAU Symp. 186, Galaxy Interactions at Low and High Redshift, ed. J. E. Barnes & D. B. Sanders (Dordrecht: Kluwer), 1
Schweizer, F., Whitmore, B. C., & Rubin, V. C. 1983, AJ, 88, 909
Swaters, R. A., & Rubin, V. C. 2003, ApJ, 587, L23
Toomre, A., & Toomre, J. 1972, BAAS, 4, 214
van der Marel, R., & Franx, M. 1993, ApJ, 407, 525
Wagner, S. J., Bender, R., & Moellenhoff, C. 1988, A&A, 195, L5
Whitmore, B. C., McElroy, D. B., & Schweizer, F. 1987, ApJ, 314, 439
Wozniak, H., Combes, F., Emsellem, E., & Friedli, D. 2003, A&A, 409, 469
Wozniak, H., Friedli, D., Martinet, L., Martin, P., & Bratschi, P. 1995, A&AS, 111, 115
Ziegler, B. L., & Bender, R. 1997, MNRAS, 291, 527